

Estimation of fault-zone conductance by calibration of a regional groundwater flow model: Desert Hot Springs, California

Alex Mayer · Wesley May · Chad Lukkarila ·
Jimmy Diehl

Abstract The hydraulic conductance of a large fault zone has been estimated by calibrating a regional groundwater flow model. Drops in groundwater elevations of over 80 m have been observed along a 15-km length of the Mission Creek fault, California, USA. The large drops in elevation are attributed to the reduced hydraulic conductivity of the fault materials. A conceptual and numerical model of the two hydrologic subbasins in Desert Hot Springs, separated by the Mission Creek fault, was developed. The model was used to estimate the hydraulic conductance along the fault. The parameter estimation involved calibrating the model with observed groundwater elevations from over 40 locations over a 60-year period. The fault hydraulic conductances were estimated assuming a linear trend in the fault length, yielding variations in the fault hydraulic conductance of about an order of magnitude along the fault length (2×10^{-11} – 4×10^{-10} 1/s). When an average fault thickness of 35 m is assumed, the fault hydraulic conductivity values are estimated to be from three to five orders of magnitude lower than the surrounding materials. A sensitivity analysis indicated that assumptions made in the conceptual model do not significantly affect estimated fault hydraulic conductances.

Résumé La conductance hydraulique d'une zone présentant une large faille a été estimée grâce à la calibration d'un

modèle hydrogéologique régional d'écoulement. Des chutes de niveaux piézométriques de plus de 80 m ont été observées le long de la faille de Mission Creek en Californie, Etats-Unis, sur une longueur de 15 km. Les importantes baisses de niveau sont attribuées à la faible conductivité hydraulique des matériaux de la faille. Un modèle conceptuel et numérique des deux sous-bassins hydrologiques du Desert Hot Springs, séparés par la faille de Mission Creek a été élaboré. Le modèle a été utilisé pour estimer la conductance hydraulique le long de la faille. L'estimation de ce paramètre a impliqué de calibrer le modèle avec les niveaux piézométriques observés au niveau de 40 localisations sur une période de 60 ans. Les conductances hydrauliques de la faille ont été estimées avec l'hypothèse d'une tendance linéaire sur la longueur de la faille, accommodant les variations des valeurs de conductance hydraulique de la faille d'environ un ordre de grandeur le long de la longueur de la faille (2×10^{-11} – 4×10^{-10} s⁻¹). Lorsque l'épaisseur moyenne de la faille est supposée de 35 m, les valeurs de conductivité hydraulique de la faille sont estimées être entre 3 à 5 ordres de grandeurs inférieurs par rapport aux matériaux environnants. Une analyse de sensibilité a indiqué que les hypothèses formulées dans le modèle conceptuel n'affectent pas de manière significative les conductances hydrauliques estimées de la faille.

Resumen Se ha estimado la conductancia hidráulica de una gran zona de falla, mediante la calibración de un modelo de flujo regional de agua subterránea. Se han observado caídas en las elevaciones del agua subterránea por encima de 80 m a lo largo unos 15-km de longitud de la falla Mission Creek, California, EE.UU. Se atribuyen los descensos grandes en la elevación, a la conductibilidad hidráulica reducida de los materiales de la falla. Se desarrollaron un Modelo conceptual y numérico de las dos subcuencas hidrológicas en el Desierto Hot Springs, separadas por la falla de Misión Creek. El modelo fue utilizado para estimar la conductancia hidráulica a lo largo de la falla. La estimación del parámetro involucró calibrar al modelo, con las elevaciones del agua subterránea observadas en más de 40 localidades y por un periodo mayor a 60 años. Las conductancias hidráulicas de la falla se estimaron asumiendo una tendencia lineal en la longitud de la falla, obteniendo variaciones en la conductancia hidráulica de la falla, de alrededor de un orden

Received: 14 December 2005 / Accepted: 5 January 2007
Published online: 10 February 2007

© Springer-Verlag 2007

A. Mayer (✉) · J. Diehl
Department of Geological and Mining Engineering and Sciences,
Michigan Technological University,
1400 Townsend Drive,
Houghton, MI 49931, USA
e-mail: asmayer@mtu.edu
Tel.: +1-906-4873372
Fax: +1-906-4873371

W. May
Arcadis,
126 N. Jefferson St., Suite 400,
Milwaukee, WI 53202, USA

C. Lukkarila
Kleinfelder and Associates,
2405 140th Ave NE, Suite A101,
Bellevue, WA 98005, USA

de magnitud a lo largo de la longitud de la falla (2×10^{-11} – $4 \times 10^{-10} \text{ s}^{-1}$). Cuando es supuesto un espesor medio de la falla de 35 m, se estiman los valores de conductibilidad hidráulicos de la falla, de tres a cinco órdenes de magnitud más bajos que los de materiales circundantes. Un análisis de sensibilidad indicó, que los supuestos hechos en el modelo conceptual, no afectan significativamente las conductancias hidráulicas estimadas de la falla.

Keywords Faults · Hydraulic properties · Inverse modeling · Regional model · Unconsolidated sediments

Introduction

Faults that act as barriers can appreciably affect groundwater-flow patterns at the basin or regional scale (e.g., Smith et al. 1990; Bredehoeft et al. 1992; Haneberg 1995; Lopez and Smith 1996). The degree to which a particular fault impedes groundwater flow depends on the materials found in the fault zone, the type and distribution of adjacent aquifer materials, and the occurrence of diagenesis in the fault zone, as well as the externally imposed flow regime (Heynekamp et al. 1999). Almost all investigations of faults that act as barriers to subsurface fluid flow have been conducted in well-lithified materials. However, as noted by Heynekamp et al. (1999), faulted, poorly lithified sediments constitute many of the most important aquifers in the southwestern US and elsewhere in the arid to semi-arid parts of the world.

Mechanical and chemical processes have been associated with the reduction of hydraulic conductivity in unconsolidated sediments in fault zones, including (1) cataclasis, or grain-size reduction, (2) offsetting of permeable beds by impermeable beds, (3) rotation of elongated and flat clasts parallel with the fault surface, reducing the hydraulic conductivity perpendicular to the fault, (4) tectonic mixing or smearing of beds of low hydraulic conductivity sediments (i.e., clays) in the fault zone, and (5) deposition of minerals in the fault zone, reducing the pore space and, hence, the hydraulic conductivity (Mozley and Goodwin 1995; Mozley et al. 1995; Mozley and Davis 1996; Caine et al. 1996; Sigda et al. 1999; Caine and Forster 1999; Heynekamp et al. 1999; Bense et al. 2003). Although advances are being made in understanding the small-scale processes contributing to reductions in the hydraulic conductivity of unconsolidated fault material, few data are available on the hydraulic parameters that are needed for regional hydrologic studies of faulted aquifers (Marler and Ge 2003).

Although very large drops in groundwater elevations and other evidence of faults acting to impede groundwater flow have been reported in field studies (e.g., Huntoon and Lundy 1979; Ganser 1987; Huntoon 1985; Kolm and Downey 1994), these studies have not yielded estimates of the fault-zone hydraulic conductivity. The usual assumption is that faults are homogeneous along their length and are usually treated as no-flow boundaries in numerical models. Because this assumption is rarely verified, little

information is available on the basic hydraulic properties and distribution of fault materials.

The availability of groundwater resources in faulted, unconsolidated basins can depend on the hydraulic properties of the faults. For example, in the arid area investigated in this study (Desert Hot Springs, California), further development depends on the availability of groundwater in the local subbasin. This subbasin is separated from another subbasin by a fault. Because recharge from local precipitation is very small (less than 13 cm annually on the valley floor), the amount of water contributed across the fault could form a significant portion of the overall recharge to the aquifer in the local subbasin. Water quality also can be affected by the hydraulic properties of faults that separate aquifers with higher quality water from those with lower quality water. This result is again the case in the area investigated in this study, where high concentrations (concentrations above water-quality standards) of hazardous compounds associated with natural and anthropogenic sources are found on one side of the fault, but not the other. The flux of these compounds across the fault into the subbasin with higher quality water is directly related to the magnitude of flow across the fault.

The purpose of this work is to estimate the macroscopic, hydraulic properties of a large, high-displacement fault zone in an unconsolidated aquifer. The hydraulic properties of the fault zone are estimated by inverse modeling, whereby a regional-scale, groundwater-flow model is calibrated with groundwater elevations collected from over 40 locations over six decades. Multiple hydrogeologic parameter values are estimated by minimizing a weighted least-squares objective function that accounts for measurement error. The quality of the estimated parameters is assessed by determining confidence intervals and testing for covariance between parameters. A sensitivity analysis was conducted to assess the significance of key assumptions made in developing the conceptual model; specifically, the assumption that outflow rates remain constant over the study period and the rate of pumped water returned to the subsurface.

Description of study area

The study area is situated around the city of Desert Hot Springs, Riverside County, California in the upper Coachella Valley (see Fig. 1). The upper Coachella Valley is filled with alluvium, with estimates of depths to underlying bedrock of more than 1 km (Proctor 1968). The upper Coachella Valley has a tropical desert climate. Annual temperatures vary from 49°C during the summer to below 0°C during the winter (Proctor 1968). The average annual precipitation is from 76 to 102 cm in the mountains and less than 13 cm on the valley floor (Harding Lawson Associates 1985).

The San Bernardino Mountains and Indio Hills bound the study area to the west and east, respectively. The study area is bounded to the north by the Little San Bernardino Mountains and to the south by the Banning fault, an extension of the San Andreas fault system. Another

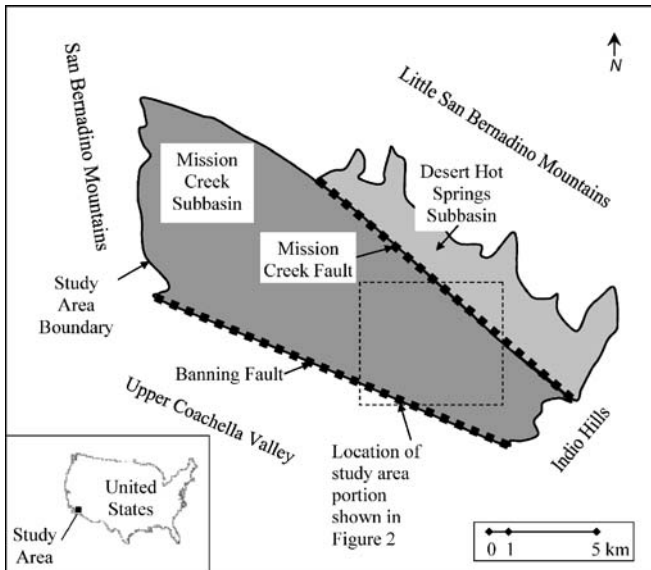


Fig. 1 Study area location in California, and map showing faults and subbasins

branch of the San Andreas fault system, the Mission Creek fault, bisects the study area to form the Desert Hot Springs subbasin to the north of the fault, and the Mission Creek subbasin to the south. Both the Banning and Mission Creek faults are right lateral reverse faults, dipping 80–90° to the northeast (Proctor 1968). The faults can be traced across the ground surface of the study area

by the appearance of vegetation, topographic scarps, and disrupted alluvium (see Fig. 2).

The study focused on a 15-km section of the Mission Creek fault (see Fig. 1), where observations indicate that the fault, or fault zone, is acting as a barrier to groundwater flow. Proctor (1968) first suggested that the presence of phreatophytic vegetation (plants that extract water from water tables via their root system) along the northern side of the Mission Creek fault trace (see Fig. 2) was an indication of high groundwater elevations. Proctor (1968) further surmised that the high groundwater elevations were caused by the fault impeding fluid flow. Measured differences in groundwater levels of more than 80 m across the fault zone have been reported (California Department of Water Resources 1964; May 1996; Lukkarila 1999), yielding apparent hydraulic gradients of greater than 10% across (perpendicular to the strike of) the fault zone. A distinct difference in the chemistry and temperature of the groundwater on either side of the fault also indicates very low flow rates across the Mission Creek fault (Geotechnical Consultants 1979; Proctor 1968). The mechanism responsible for impeding groundwater flow across the Mission Creek fault is not understood, although cementation is suspected to have created a low hydraulic conductivity zone (Harding Lawson Associates 1985; May 1996). Zones of cemented materials have been observed in sediments exposed in road cuts and excavations (Harding Lawson Associates 1985; May 1996).

Fig. 2 Aerial photo of a portion of the study area, including indication of faults (white dotted lines) and vegetation scarps

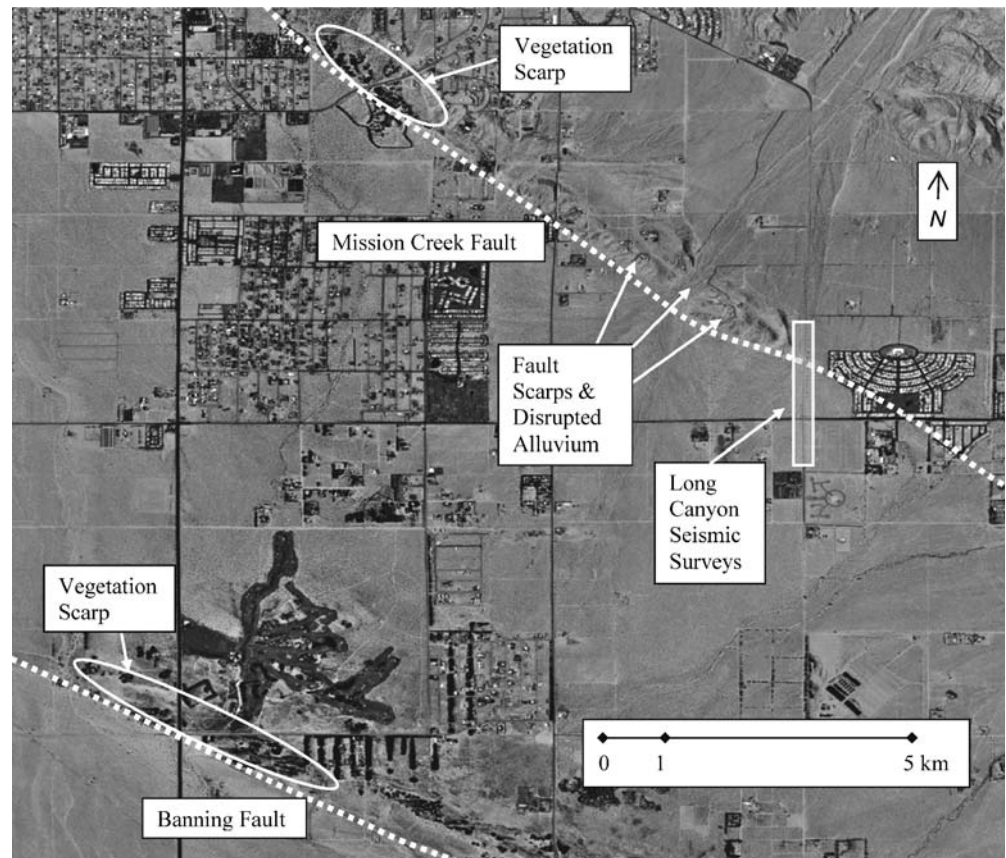


Figure 3 shows groundwater-elevation contours from a set of measurements collected in 1998; Fig. 4 shows ground-surface elevations for reference. The general direction of groundwater flow in the subbasins is primarily along the northwest to southeast axis of the valley, a pattern consistent with the regional pattern in the upper Coachella Valley (Tyley 1971). The exception to the pattern is the bend towards the southern end of the Banning fault. The steep gradient across the Mission Creek fault zone is implied by the large differences in measured groundwater elevations on either side of the fault.

In general, there is a distinct contrast between the chemistry and temperature of the groundwater in the two subbasins (Geotechnical Consultants 1979, 1992). The groundwater in the Desert Hot Springs subbasin has a geothermal character, with total dissolved solids (TDS) concentrations of over 1,000 mg/L and temperatures exceeding 50°C. The groundwater chemistry in the majority of the Desert Hot Springs subbasin has been characterized as predominately Ca–Na₂CO₃–SO₄ (Geotechnical Consultants 1979).

The groundwater in the Mission Creek subbasin is similar in character to groundwater in the upper Coachella Valley, with TDS concentrations of 100–500 mg/L, temperatures of 30–35°C, and chemistry characterized as predominately Na–SO₄. However, along the southeastern section of the Mission Creek fault, between Long Canyon (see Fig. 5) and the southeastern end of the study area, the groundwater chemistry in the Mission Creek subbasin is characterized as Na–SO₄, and TDS concentrations ranging between 500 and 900 mg/L are found (Geotechnical Consultants 1979).

Groundwater-model development

Groundwater models have been developed in and around the study area as part of groundwater-resource assessments

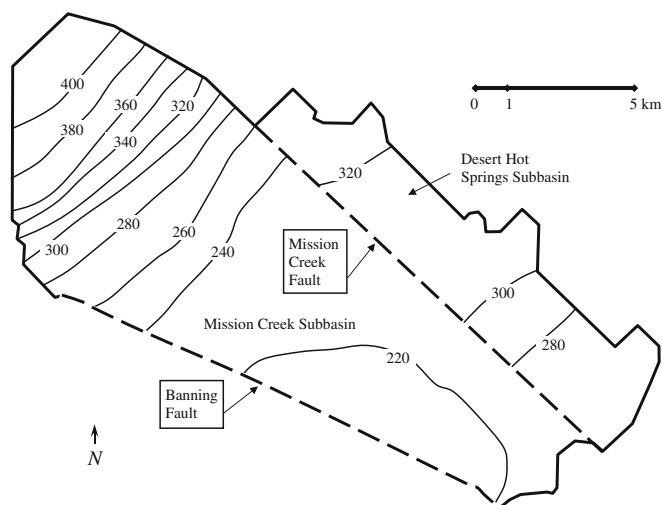


Fig. 3 Observed groundwater elevations in meters above mean sea level, 1998. Groundwater elevations used in this figure consist of water-level measurements taken from observation wells and elevations determined from electrical resistivity surveys

(Tyley 1971, 1974; Swain 1978; Reichard and Meadows 1992). In each of these investigations, the Mission Creek fault zone was treated as a complete barrier to groundwater flow in order to simplify the modeling efforts. In this work, a conceptual and numerical groundwater-flow model was developed for the Desert Hot Springs area, where the Mission Creek fault zone has non-zero hydraulic conductance. The model is used to estimate the fault conductance, along a 15-km section of the fault zone, via a two-phase calibration and verification procedure.

Conceptual model

The groundwater system is treated as a single layer aquifer under unconfined conditions. The aquifer materials are composed of the Pleistocene Cabezon fanglomerate and Ocotillo conglomerate. These materials are poorly sorted and poorly consolidated, consisting of coalescing alluvial fan, braided stream, and debris flow deposits (California Department of Water Resources 1964). No laterally continuous units can be identified from lithologic logs from well-installation records, which are separated on the order of hundreds of meters to kilometers. The apparent lack of correlation at this scale for this study has led to the application of a hydraulic conductivity distribution model that is homogeneous in the vertical and distributed in blocks in the aerial direction.

The lateral boundaries of the study area are shown in Fig. 5. The northern and western boundaries, which generally follow the outline of the San Bernardino and Little San Bernardino Mountains, are treated as no-flow boundaries, except where canyons intersect the boundary and subsurface inflow occurs. Portions of the boundaries to the southeast coincide with the Indio Hills, which are composed of the Palm Springs Formation and consist of semiconsolidated siltstones, claystones, and sandstones (California Department of Water Resources 1964). It was assumed that this material creates a no-flow boundary on the southeastern corner of the study area (Proctor 1968). Outflow of groundwater from the study area occurs via (1)

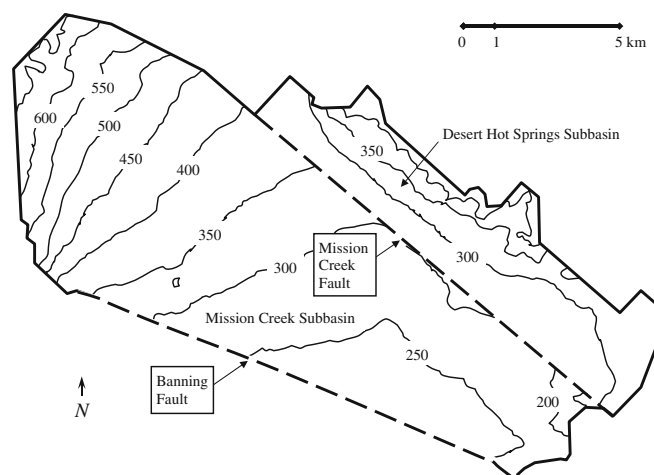


Fig. 4 Ground-surface elevations in meters above mean sea level (contour interval 50 m)

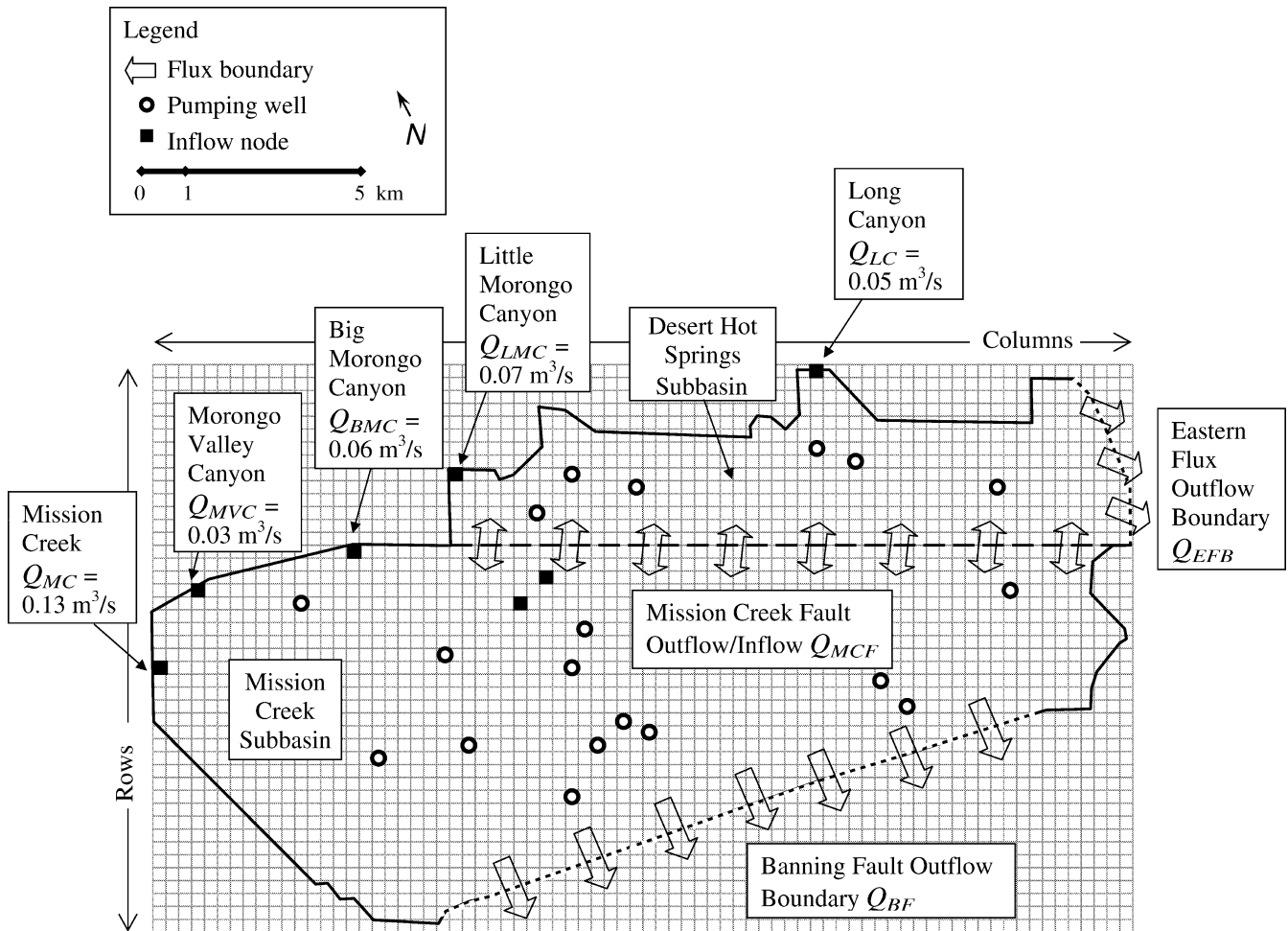


Fig. 5 Location of inflow and outflow boundary conditions and estimates of inflows from Tyley (1971); locations of pumping wells; and finite-difference grid used in model simulations

groundwater flow across the Banning Fault, (2) groundwater outflow through an area to the north of the Indio Hills (“eastern flux boundary”), and (3) evapotranspiration through phreatophytes on the ground surface near the Banning or Mission Creek fault. The outflow locations are indicated in Fig. 5.

The basement rock in the upper Coachella Valley area consists of the San Geronio igneous-metamorphic complex (California Department of Water Resources 1964). Proctor (1968) suggests that typical sediment thicknesses in the upper Coachella Valley are greater than 400 m. However, recent seismic refraction and reflection surveys at Long Canyon (see Fig. 2 for location) indicate that low hydraulic conductivity materials could be as near as 70 m below ground surface on the Desert Hot Springs subbasin side of the Mission Creek fault (R. Catchings, US Geological Survey, unpublished data, 1999).

Surface-water flow in the study area consists of ephemeral or intermittent streams that originate in the mountains. Mission Creek is the only stream that flows to the valley floor on a consistent basis, but the stream usually disappears a short distance from its entrance into the study area. Streams flowing through Morongo Valley,

Big Morongo, Little Morongo, and Long Canyons periodically reach the valley floor for short periods of time when there are localized, intense storms in the mountains. The water recharging the aquifer originates as precipitation in the mountains forming the northern and western boundaries and enters the study area almost exclusively as subsurface inflow via the major canyons.

The study period began in 1936, since, according to Tyley (1971), nearly steady-state conditions were present in the upper Coachella Valley, because very little pumping occurred at this time and historical records indicate an average precipitation year for the area. Figure 5 shows the locations of inflows and outflow and the corresponding rates estimated by Mayer and May (1998), based on the rates estimated by Tyley (1971) for the year 1936. Tyley (1971) estimated the inflows and outflows by using a combination of precipitation estimates and water balances.

Given the inflows and outflows described above, the water balances for the two subbasins are proposed as

$$\text{Desert Hot Springs subbasin :} \quad Q_{LMC} + Q_{LC} = Q_{MCF} + Q_{EFB} + P_{DHS} + \Delta S_{DHS}, \quad (1a)$$

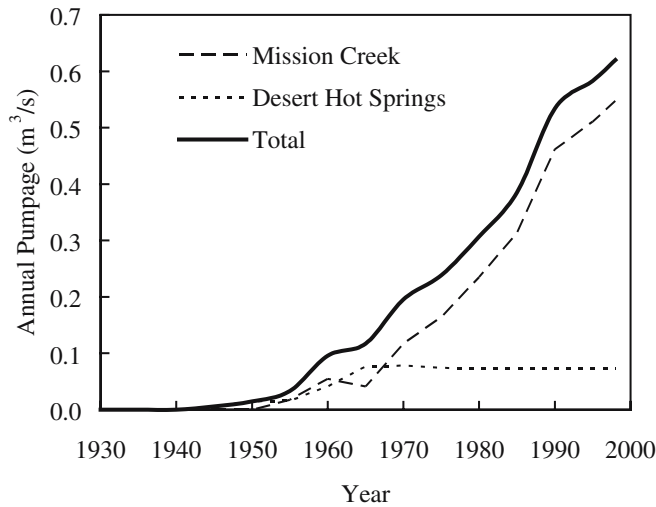


Fig. 6 Annual pumpage from study area for *Desert Hot Springs* and *Mission Creek* subbasins

Mission Creek subbasin :

$$Q_{MC} + Q_{MVC} + Q_{BMC} + Q_{MCF} = Q_{BF} + P_{MC} + \Delta S_{MC}, \tag{1b}$$

where Q_{LMC} is the inflow from Lower Morongo Canyon, Q_{LC} is the inflow from Long Canyon, Q_{MCF} is the flow across the Mission Creek fault, Q_{EFB} is the outflow from the eastern flux boundary, Q_{MC} is the inflow from Mission Creek, Q_{MVC} is the inflow from Morongo Valley Canyon, Q_{BMC} is the inflow from Big Morongo Valley Canyon, Q_{BF} is the outflow across the Banning fault (see Fig. 5), P_{DHS} and P_{MC} are the pumping rates in the Desert Hot Springs and Mission Creek subbasins, respectively, and ΔS_{DHS} and ΔS_{MC} are the storage changes in the Desert Hot Springs and Mission Creek subbasins, respectively. Figure 5 shows the locations of the inflows and outflows and the estimates for the inflows provided by Tyley (1971).

Evapotranspiration through phreatophytes along portions of the fault zone also was considered. Calculated values of evapotranspiration for the Banning and Mission Creek faults are 0.032 and 0.0012 m³/s, respectively, using an aerial evapotranspiration rate from Lines and Bilhorn (1996) for similar vegetation (1.3×10^{-8} m³/s/m²). The evapotranspiration at the Mission Creek is negligible and is ignored in the conceptual and numerical models. The evapotranspiration at the Banning fault is lumped into the Banning fault outflow rate.

The net annual pumpage from the Desert Hot Springs and Mission Creek subbasins is shown in Fig. 6. Most of the pumping in the study area occurs near the city of Desert Hot Springs. Approximately 20% of the pumped groundwater is transported out of the study area. The remainder of the pumped groundwater is used in the study area and is either returned to the subsurface through irrigation and sewage-effluent return or is lost to evapotranspiration or other sinks. It is assumed that, on average, 35% of the pumped groundwater is returned to the subsurface (Tyley 1971). The significance of this assumption is assessed in the sensitivity analysis section.

Numerical model

Assuming that the fluid density is constant, the principal axes of hydraulic conductivity are aligned with the coordinate directions, and the aquifer is homogeneous and isotropic, the vertically averaged groundwater flow equation is (Bear 1979)

$$\frac{S}{T} \frac{\partial h}{\partial t} = \frac{\partial^2 h}{\partial x^2} + \frac{\partial^2 h}{\partial y^2} - W, \tag{2}$$

where S is the storage coefficient, $T=Kh$ is the transmissivity along the x and y coordinate axes, $h=H-z_{bot}$ is the potentiometric elevation above the aquifer bottom, H is the potentiometric elevation AMSL (above mean sea level), z_{bot} is the elevation of the aquifer bottom AMSL,

Table 1 Parameter best estimates and Confidence Intervals (CI)

| Parameter, inflow, or outflow | Variable | Prior estimate | Steady-state calibration | | Transient calibration | | Units |
|-----------------------------------|-----------|----------------|--------------------------|-----------------------|-----------------------|-----------------------|---------------------|
| | | | Best estimate | 95% CI | Best estimate | 95% CI | |
| Mission Creek inflow | Q_{MC} | 0.13 | 0.13 | 0.16 | 0.04 | 0.15 | m ³ /s |
| Morongo Valley Canyon inflow | Q_{MVC} | 0.03 | 0.03 | 0.05 | 0.02 | 0.06 | m ³ /s |
| Big Morongo Canyon inflow | Q_{BMC} | 0.06 | 0.06 | 0.04 | 0.02 | 0.04 | m ³ /s |
| Little Morongo Canyon inflow | Q_{LMC} | 0.07 | 0.07 | 0.06 | 0.03 | 0.10 | m ³ /s |
| Long Canyon inflow | Q_{LC} | 0.05 | 0.05 | 0.04 | 0.02 | 0.08 | m ³ /s |
| Eastern flux boundary outflow | Q_{EFB} | 0.07 | 0.07 | 0.05 | 0.02 | 0.06 | m ³ /s |
| Banning fault outflow | Q_{BF} | 0.27 | 0.27 | 0.30 | 0.06 | 0.18 | m ³ /s |
| Storage coefficient | S | NA | NA | NA | 0.12 | 0.03 | - |
| Transmissivity Desert Hot Springs | a_{DHS} | NA | -6.4×10^{-7} | 2.3×10^{-7} | -7.7×10^{-7} | 2.8×10^{-7} | m ² /s/m |
| $T_{DHS} = a_{DHS}x + b_{DHS}$ | b_{DHS} | NA | 3.4×10^{-2} | 6.7×10^{-3} | 2.5×10^{-2} | 4.9×10^{-3} | m ² /s |
| Transmissivity Mission Creek | a_{MC} | NA | -1.5×10^{-7} | 5.0×10^{-8} | -1.8×10^{-7} | 5.4×10^{-8} | m ² /s/m |
| $T_{MC} = a_{MC}x + b_{MC}$ | b_{MC} | NA | 2.4×10^{-3} | 6.0×10^{-4} | 2.9×10^{-3} | 5.8×10^{-4} | m ² /s |
| Fault Conductance | a_F | NA | 3.1×10^{-14} | 6.0×10^{-15} | 2.4×10^{-14} | 4.8×10^{-15} | 1/s/m |
| $K^* = a_Fx + b_F$ | b_F | NA | 1.7×10^{-11} | 8.7×10^{-12} | 2.2×10^{-11} | 1.0×10^{-11} | 1/s |

NA not applicable

CI confidence interval

Table 2 Estimates of uncertainties associated with model inputs and measurements used in calibration procedure

| Calibration phase | Input/measurement | Uncertainty | Methodology used to estimate uncertainty |
|--------------------------|---|-------------|---|
| Steady-state calibration | Water levels interpolated from Tyley (1971) potentiometric-surface map | 0.20 m | Assumed |
| Transient calibration | Groundwater-elevation observations from local water-agency records over the period 1937–1998 | 0.10 m | Assumed |
| | Water levels estimated from wells in May (1996) and Lukkarila (1999) less measurements taken at fault transects | 0.05 m | Precision: estimated from repeated measurements in a single well |
| | Water levels estimated from resistivity surveys in Lukkarila (1999) less measurements taken at fault transects | 0.13 m | Accuracy: average difference between water levels estimated from wells and resistivity surveys (taken at the same location) |
| | | 0.24 m | Precision: estimated from repeated measurements at a single location |
| | | 0.37 m | Sum of accuracy and precision |

K is the hydraulic conductivity, and W is a volumetric flux per unit area and represents sources or sinks of water. The assumption of constant fluid density ignores the significant differences in temperature and concentrations of dissolved solids in groundwater across the study area. However, a maximum density difference of less than 1% is associated with the extremes in temperature (30–55°C) and dissolved solids concentrations (100–1,500 mg/L). This density difference is not expected to appreciably affect the processes considered in this study.

The numerical model used for this study is MODFLOW, a well-known, quasi-three-dimensional groundwater-flow modeling program (McDonald and Harbaugh 1988) based on Eq. (2). The MODFLOW horizontal flow barrier (HFB) package was utilized here (Hsieh and Freckleton 1993) to simulate the effect of the Mission Creek fault on groundwater flow. The HFB package essentially simulates the fault via a leakance term between two horizontally adjacent finite-difference cells. The HFB package is based on the assumption that the fault is vertically oriented and that the flow through the adjacent cells is horizontal. The fault hydraulic properties are input as a conductance, $K^* = K_f/c$, where K_f and c are the fault

hydraulic conductivity and thickness in the direction normal to flow, respectively.

The numerical model is based on a single layer, 170-column \times 98-row rectangular grid, that is oriented along the strike of the Mission Creek fault (see Fig. 5). Only 9,643 cells are active, due to the irregular boundary of the study area. Each cell is 125 \times 125 m. Inflows are simulated as constant-flux terms at the relevant grid cells (see Fig. 5 for location), as are the outflows along the Banning fault and the eastern flux boundary. All other grid cells along the boundary are no-flow. Pumping rates at 21 wells are represented in the model grid and are based on historical pumpage records, beginning in 1936 (see Fig. 5 for location and Fig. 6 for an illustration of the pumping rates).

Model calibration, verification, and sensitivity analysis

The model calibration consisted of two phases: a steady-state calibration based on observations collected in a year (1936), where little or no pumping occurred, and a

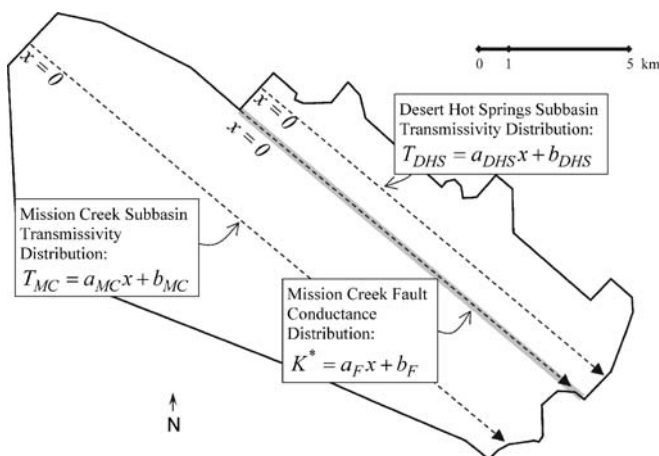


Fig. 7 Assumed directions of transmissivity patterns for the Desert Hot Springs and Mission Creek subbasins and assumed directions of fault conductance patterns

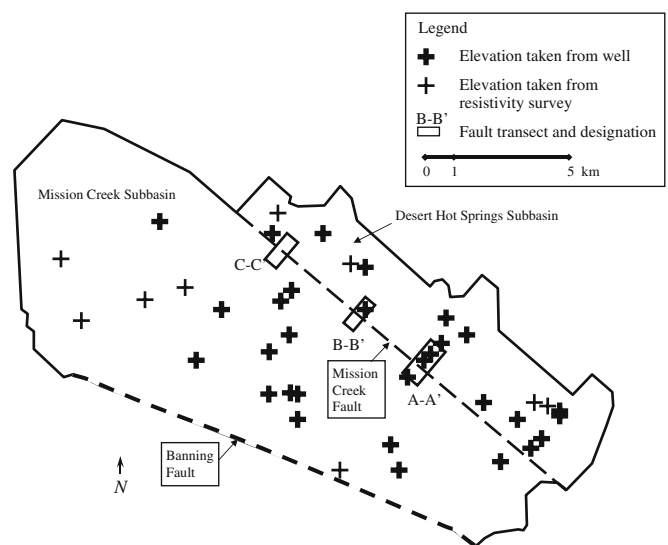


Fig. 8 Location of groundwater-elevation measurement points and fault transects. Note that not all individual measurement points are indicated in the fault transects

Table 3 Cross-correlation matrix for estimated parameters fro transient calibration

| | Q_{MC} | Q_{MVC} | Q_{BMC} | Q_{LMC} | Q_{LC} | Q_{EFB} | Q_{BF} | S | a_{DHS} | b_{DHS} | a_{MC} | b_{MC} | a_F | b_F |
|-----------|----------|-----------|-----------|-----------|----------|-----------|----------|-------|-----------|-----------|----------|----------|-------|-------|
| Q_{MC} | 1.00 | | | | | | | | | | | | | |
| Q_{MVC} | -0.77 | 1.00 | | | | | | | | | | | | |
| Q_{BMC} | -0.54 | 0.57 | 1.00 | | | | | | | | | | | |
| Q_{LMC} | -0.03 | -0.13 | 0.15 | 1.00 | | | | | | | | | | |
| Q_{LC} | -0.03 | -0.10 | 0.10 | -0.45 | 1.00 | | | | | | | | | |
| Q_{EFB} | -0.03 | -0.06 | 0.07 | 0.48 | 0.33 | 1.00 | | | | | | | | |
| Q_{BF} | 0.35 | 0.39 | 0.23 | -0.03 | 0.03 | -0.17 | 1.00 | | | | | | | |
| S | 0.29 | 0.34 | -0.28 | 0.39 | 0.41 | 0.44 | -0.39 | 1.00 | | | | | | |
| a_{DHS} | 0.00 | 0.06 | -0.03 | 0.06 | -0.04 | -0.06 | 0.00 | 0.07 | 1.00 | | | | | |
| b_{DHS} | -0.01 | -0.09 | 0.10 | -0.19 | 0.22 | 0.29 | -0.08 | -0.04 | 0.44 | 1.00 | | | | |
| a_{MC} | -0.05 | -0.07 | 0.10 | 0.06 | 0.08 | 0.00 | -0.06 | 0.00 | 0.00 | -0.03 | 1.00 | | | |
| b_{MC} | 0.15 | 0.18 | 0.10 | -0.08 | -0.10 | -0.03 | 0.19 | -0.01 | 0.04 | 0.03 | -0.47 | 1.00 | | |
| a_F | 0.08 | -0.06 | -0.09 | -0.11 | 0.01 | -0.05 | 0.08 | 0.03 | 0.07 | 0.05 | 0.03 | 0.01 | 1.00 | |
| b_F | -0.03 | -0.09 | 0.12 | -0.18 | 0.18 | 0.10 | -0.17 | -0.03 | -0.05 | -0.03 | -0.11 | -0.01 | -0.38 | 1.00 |

transient calibration based on observations from 1937 through 1998. A separate data set collected in the vicinity of the fault zone was used to verify the model. Finally, sensitivity to basic assumptions in the conceptual model conceptual was assessed.

Inflow and outflow rates, transmissivities, storativity, and fault conductances were estimated via model calibration. The parameters estimated by calibration are listed in Table 1, along with prior estimates of the parameters. Prior estimates for inflows and outflows were obtained as described previously in the conceptual model section. The “observations” used in the calibration procedure consist of published maps of groundwater elevations, historical groundwater-elevation records from public water supply wells, direct measurements of groundwater elevations in observation wells, and groundwater elevations interpreted from electrical resistivity surveys. It was assumed that the “observed” groundwater elevations are equivalent to the vertically averaged hydraulic heads predicted by the model at the corresponding nodal location. Uncertainty estimates for each category of observed groundwater elevations are provided in Table 2.

Best parameter estimates were found using the PEST package for nonlinear parameter estimation (Doherty 1994). The PEST package is based on the Gauss-Marquardt-Levenberg method. The objective of the parameter estimation is to find the minimum global sum of the squares of the residuals (SSR) between the observations and the model predictions, as in

$$SSR = \sum_{i=1}^N (h_i^{model} - h_i^{obs})^2 \tag{3}$$

where N is the number of observations and h^{model} and h^{obs} are the groundwater elevations obtained from model simulations and from observations, respectively. Optimum parameter values are constrained to lie between individually specified upper and lower bounds. The uniqueness and optimality of the parameter estimates were tested by repeating the calibrations using a wide range of starting points for the parameter estimates.

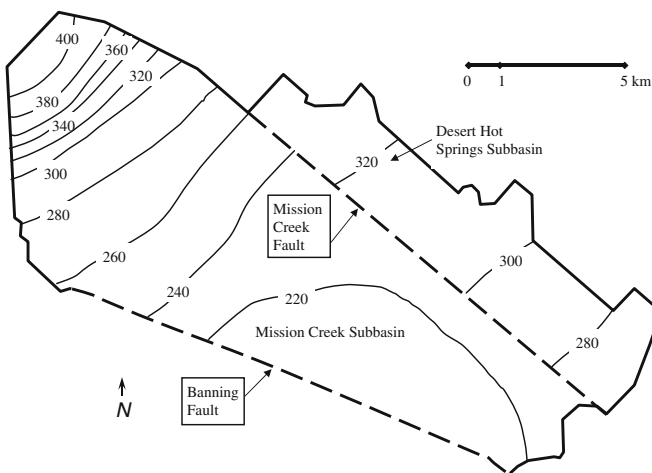


Fig. 9 Simulated groundwater elevations in meters above mean sea level, 1998

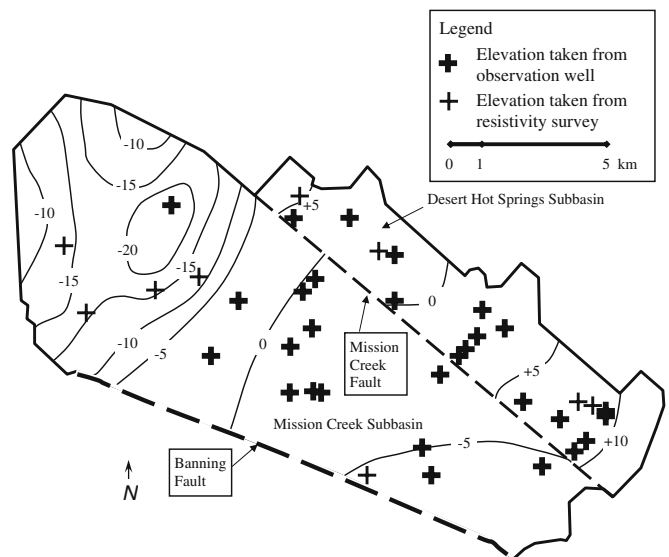


Fig. 10 Residuals between simulated and observed groundwater elevations (simulated minus observed elevations) in meters, 1998

Table 4 Water-balance after transient Calibration, 1998

| Water-balance component | Quantity | Units |
|---|----------|-------------------|
| Mission Creek subbasin | | |
| Mission Creek inflow | 0.15 | m ³ /s |
| Morongo Valley Canyon inflow | 0.06 | m ³ /s |
| Big Morongo Canyon inflow | 0.04 | m ³ /s |
| Mission Creek fault (in) | 0.07 | m ³ /s |
| Mission Creek subbasin total inflow | 0.32 | m ³ /s |
| Banning fault outflow | 0.18 | m ³ /s |
| Mission Creek subbasin pumpage | 0.36 | m ³ /s |
| Mission Creek subbasin total outflow | 0.54 | m ³ /s |
| Mission Creek subbasin change in storage as volume | -0.22 | m ³ /s |
| Mission Creek subbasin change in storage as groundwater elevation ^a | -0.52 | m/year |
| Desert Hot Springs subbasin | | |
| Little Morongo Canyon inflow | 0.10 | m ³ /s |
| Long Canyon inflow | 0.08 | m ³ /s |
| Desert Hot Springs subbasin total inflow | 0.18 | m ³ /s |
| Eastern flux boundary outflow | 0.06 | m ³ /s |
| Mission Creek fault (out) | 0.07 | m ³ /s |
| Desert Hot Springs subbasin pumpage | 0.05 | m ³ /s |
| Desert Hot Springs subbasin total outflow | 0.18 | m ³ /s |
| Desert Hot Springs subbasin change in storage as volume | 0.00 | m ³ /s |
| Desert Hot Springs subbasin change in storage as groundwater elevation ^a | -0.01 | m/year |

^a Change in groundwater level calculated as (change in storage as volume)/(area) (storage coefficient)

Variances were assigned to all observations. The variances were assumed to reflect the uncertainty given in Table 2. Equation (3) was modified to separate the SSRs associated with each category of measurement. The individual SSRs are weighted by the inverse of the variances as in the following example, where observations from observation well measurements (subscript “ow”) are combined with groundwater elevations estimated from resistivity surveys measurements (subscript “rs”) yielding

$$SSR = \frac{1}{\sigma_{ow}^2} \sum_{i_{ow}=1}^{N_{ow}} (h_{i_{ow}}^{model} - h_{i_{ow}}^{obs})^2 + \frac{1}{\sigma_{rs}^2} \sum_{i_{rs}=1}^{N_{rs}} (h_{i_{rs}}^{model} - h_{i_{rs}}^{obs})^2 \quad (4)$$

Weighting by the inverse of the variances before the sum-of-squared residuals has the effect of giving observations less prone to error more importance in determining the parameter values.

Confidence intervals are calculated to give an indication of the uncertainty in the parameter estimates. Here, it is assumed that the true model errors are normally distributed and that the calibrated model is approximately linear with respect to the parameters near the estimated values (Seber and Wild 1989). Based on these assumptions, the individual confidence intervals are calculated as the final estimated parameter value plus or minus the product of the standard deviation of that estimate and the student *t* statistic.

The steady-state calibration phase involved estimation of inflow and outflow rates (except for the cross-fault flow Q_{MCF}), transmissivities, and fault conductances with a steady-state simulation of the year 1936. In this phase, the “observed” groundwater elevations were derived from a potentiometric-surface map from Tyley (1971). An uncertainty of 0.2 m was assumed for these values (see Table 2). Inflow and outflow rates are calibrated but are also constrained by the water balances given in Eqs. (1a) and (1b).

The transmissivity distributions in both subbasins are assumed to follow a linear trend paralleling the axis of the upper Coachella Valley, as in

$$T_{DHS} = a_{DHS}x + b_{DHS} \quad (5a)$$

$$T_{MC} = a_{MC}x + b_{MC} \quad (5b)$$

where the subscripts DHS and MC refer to the Desert Hot Springs and Mission Creek subbasins, respectively; *a* and *b* are the fitted parameters in the linear model, and *x* is the distance along the axis of the subbasins, beginning at the extreme northwestern ends of each subbasins and continuing from northeast to southeast (see Fig. 7). This pattern reflects the change in aquifer materials and depth to impermeable materials that is expected to occur in alluvium-filled valleys. Whereas the transmissivity distributions may actually follow a more complex pattern than a linear pattern, the minimal information regarding transmissivity values in the study area do not justify a more complex model.

The conductance along the Mission Creek fault also is modeled as following a linear trend:

$$K^* = a_Fx + b_F \quad (6)$$

where the subscript F refers to Mission Creek fault; *a* and *b* are the fitted parameters in the linear model, and *x* is the distance along the faults zone, beginning at the extreme northwestern end of the fault zone and continuing from northeast to southeast (see Fig. 7). The distribution of conductance along the fault zone may actually follow a more complex pattern than a linear pattern, but the minimal observation data to be used in the calibration does not justify a more complex model.

The transient calibration phase involved estimation of the storage coefficient with a transient simulation from 1937 to 1998, using the calibrated 1936 simulation as

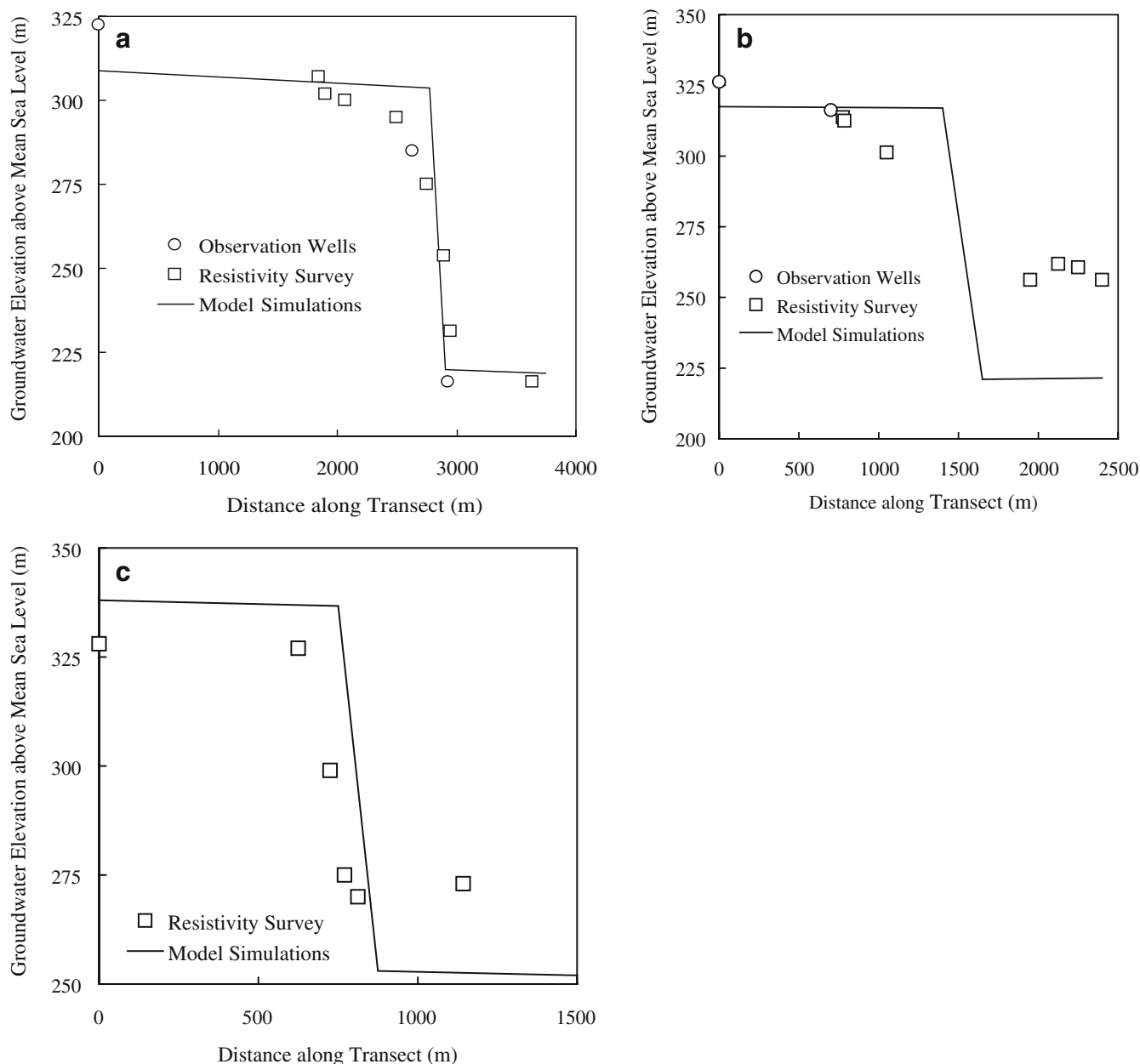


Fig. 11 Simulated and observed groundwater elevations in meters above mean sea level for fault transects in 1998: **a** transect A-A', **b** transect B-B', and **c** transect C-C'

initial conditions. The inflow and outflow rates, transmissivities, storativity, and fault conductances were also re-estimated. In this phase, groundwater-elevation observations from local water-agency records over the period from 1937 to 1998, along with measurements recently collected from 30 observation wells and 30 resistivity soundings by May (1996) and Lukkarila (1999) were used. Water levels were obtained from the observation wells using a standard depth-to-water probe. The sounding data were collected with a ABEM Terrameter SAS300B using a Schlumberger array (Zhody et al. 1974) with AB/2 spacings ranging from 3 to 200 m and MN/2 spacings from 0.4 to a maximum of 20 m. At several locations, where the depth to the water table was shallow, the

maximum AB/2 and MN/2 spacing were considerably less than listed above. The modeling program “Resist” (Vander Velpen and Sporry 1993) was used to invert the sounding data to obtain water-table depths. Root-mean-squared fits of 2–3% were generally obtained. The uncertainty for each model input and measurements is indicated in Table 2. The locations of the wells and resistivity surveys used in the calibration data sets are shown in Fig. 8.

In the verification phase, a data set of groundwater-elevation measurements collected in 1998 at three transects across the Mission Creek fault by Lukkarila (1999) was used using observation wells and resistivity surveys. The fault transect observations are compared with the 1998 model output of water levels from the transient

calibration phase. The fault transect observations are not used in either of the prior calibration phases. The locations of the three fault transects are shown in Fig. 8.

Results and discussion

Regional scale calibration

The best estimates and corresponding confidence intervals for each parameter used in regional scale calibrations are indicated in Table 1. A correlation matrix for all estimated parameters is provided in Table 3. The best estimates of the inflows and outflows are roughly similar to the prior estimates. The confidence intervals for the inflows and outflows are relatively low: on average, the confidence intervals are on the order of 25% of the best estimate values. The estimated correlations listed in Table 3, however, indicate that there is significant self-correlation between the inflows and outflows within each subbasin (but not between each subbasin). The self-correlations indicate that the ability to estimate individual inflows and outflows is relatively weak.

Figure 9 shows a contour map of simulated groundwater elevations for the year 1998, the last year of the model-simulation period. Recalling the observed groundwater elevations in Fig. 3, the simulations provide a good match with the patterns in groundwater-elevation contours. Figure 10 shows a map of the residuals between the simulated and observed groundwater elevations (simulated minus observed elevations), including the locations of the water-level observations. The highest residuals are found in the northwestern portion of the Mission Creek subbasin, where the groundwater-elevation observations are sparse.

Table 4 shows the inflows, outflows, and other flow components obtained after the transient calibration phase for the final year of the simulation (1998). These results indicate that, due to pumping rates in excess of the overall recharge rates (inflows minus outflows), there is a loss of groundwater in storage. The losses translate to significant declines in groundwater elevations in the Mission Creek subbasin (on the order of 0.5 m/year) and minimal decline in the Desert Hot Springs subbasin (on the order of 0.01 m/year). These declines are consistent with declines observed in wells in the two subbasins over the period 1990–1998.

The estimated values of the parameters in the transmissivity equations indicate that, for both subbasins, the transmissivities decrease to the southeast, or in the direction away from the mountains. This result could be explained by the expected decrease in grain size of alluvial materials as the distance from the source of the materials increases. In the Desert Hot Springs subbasin, the minimum, maximum, and average values of transmissivity are 1.7×10^{-2} , 2.5×10^{-2} , and 2.1×10^{-2} m²/s, respectively. In the Mission Creek subbasin, the minimum, maximum, and average values of transmissivity are 1.8×10^{-4} , 2.9×10^{-3} , and 1.5×10^{-3} m²/s, respectively. The higher values for the Desert Hot Springs subbasin are

likely due to the proximity of the subbasin to the mountains, indicating that the aquifer materials, on average, have higher grain sizes, and, thus, higher hydraulic conductivities.

The estimated transmissivities are a product of hydraulic conductivities and saturated thicknesses. Given that the transmissivities in the Desert Hot Springs subbasin are higher than in Mission Creek subbasin, the hydraulic conductivities are likely to be significantly higher in the Desert Hot Springs subbasin, because the saturated thicknesses are likely significantly lower in this subbasin. The lower saturated thicknesses in the Desert Hot Springs subbasin would be explained by the expected, significantly smaller depths to impermeable materials in the subbasin. Given average saturated thicknesses of 50–300 m in the Desert Hot Springs and Mission Creek subbasins, respectively, the corresponding, average hydraulic conductivities in the Desert Hot Springs and Mission Creek subbasins are 5×10^{-4} and 7×10^{-6} m/s, respectively. These values of hydraulic conductivity are within the range of expected for alluvial materials and are consistent with materials reported in lithologic logs (80% of the materials are fine to medium sands; California Department of Water Resources 1979).

A uniform value of 0.12 provided the best model fit for the storage coefficient. This value is reasonable for an aquifer under unconfined conditions consisting of unconsolidated alluvium. Spatially distributed values of the storage coefficient could not be justified, because the groundwater elevations are relatively insensitive to the storage coefficient. For example, increases or decreases of the storage coefficient by 50% resulted in changes in the sum of the squares of the residuals of less than 5%.

Calibrated fault-zone conductances

Using the values of the parameters estimated for the fault-zone conductance equation, the minimum, maximum, and average values of fault-zone conductance are 2.2×10^{-11} , 3.8×10^{-10} , and 2.0×10^{-10} 1/s, respectively. The conduc-

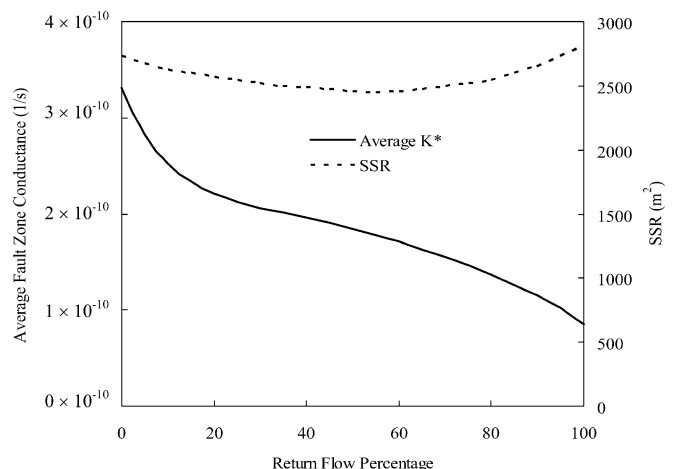


Fig. 12 Sensitivity of estimated fault conductance (averaged along fault length) and global sum of the squares of the residuals (SSR) to return flow percentage

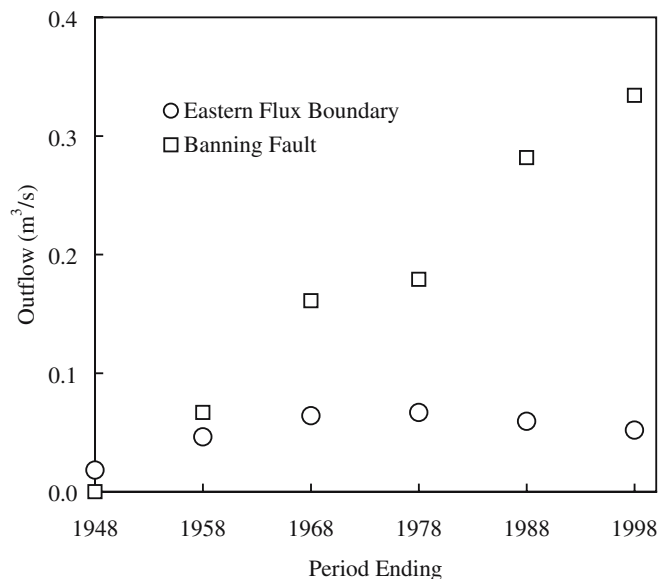


Fig. 13 Estimated, transient outflows at the eastern flux boundary and Banning fault for period ending in 10-year increments

tance values obtained for the southeastern section of the fault are about 5–10 times greater than the value for the northwestern section of the fault. This result is supported by two distinct sets of observations. First, differences in observed groundwater elevations between the two subbasins in this area are smaller in the southeastern portion of the study area, as indicated in Fig. 3. Second, as described in the description of the study area, the groundwater chemistries in the southeastern portions of the two subbasins are less distinct from each other than in the remainder of the study area. The similarity in the groundwater chemistries would indicate that there is more flow across the fault in the southeastern portion of the area, corresponding to a higher fault conductance in the area.

Given the average, estimated fault conductance (K_f/c) of 2.0×10^{-10} 1/s and assuming a constant fault-zone width (c) of 35 m (Rasmussen 1979), the fault hydraulic conductivity estimate is approximately 7×10^{-9} m/s in the northwestern to 1×10^{-8} m/s in the southeastern section. These estimated values of hydraulic conductivity are from three to five orders of magnitude lower than the calibrated, regional hydraulic conductivities in contact with the fault.

Fault-zone verification

Figure 11 shows a comparison of observed and simulated groundwater-elevation profiles across the Mission Creek

fault at three transects (see Fig. 8 for the transect locations). The observed groundwater elevations measured in the fault transects were not used in the model calibration and the simulated groundwater elevations in Fig. 11 were generated without any further parameter calibration. Figure 11a demonstrates a very good match in pattern between the observed and simulated groundwater-elevation measurements for transect A-A'.

The match is not as good as shown in Fig. 11b and c as compared to Fig. 11a. For the A-A' transect, the groundwater elevations on the upgradient side of the Mission Creek fault match well, but groundwater elevations on the downgradient side of the fault are underestimated in model simulation. The model results for transects B-B' and C-C' can be improved by increasing the hydraulic conductance of the northwestern section of the fault. However, when the fault conductance is increased, the fit over all of the observations becomes significantly worse, as measured by the global SSR.

The result described above indicates that either the parameter values local to transects B-B' and C-C' (e.g., hydraulic conductivity on the downgradient side of the fault) need to be refined or that the observed groundwater elevations obtained at the downgradient locations are erroneous. The observed groundwater elevations on the downgradient side of the fault given in Fig. 11b and c were derived exclusively from resistivity measurements. Resistivity measurements have more uncertainty than groundwater elevations measured directly from observation wells.

Sensitivity analysis

In the sensitivity analysis, the fault conductance was re-estimated as an assessment of the significance of two conceptual model assumptions: the percentage of pumped water returned is fixed, and the outflows remain constant over the period of the transient calibration. The fraction of the pumped water returned to the aquifer was assumed to be 35%. This assumption could be critical because the return flow percentage essentially controls the effective pumping rate. The return flow percentage was varied from 0% (no pumped water is returned) to 100% (all of the pumped water is returned) in steps of 5%. The transient phase calibration was repeated for each step.

The results of the sensitivity analysis are shown in Fig. 12, where the average, calibrated fault conductance (averaged along the length of the fault) is plotted against the return flow percentage. The total sums of the squares

Table 5 Comparison between constant and variable outflow approaches

| | Outflows held constant | Outflows allowed to vary | Units |
|--|------------------------|--------------------------|-------------------|
| Average eastern flux boundary outflow ^a | 0.06 | 0.05 | m ³ /s |
| Average banning fault outflow ^a | 0.18 | 0.17 | m ³ /s |
| Average fault conductance ^b | 2.0×10^{-10} | 1.8×10^{-10} | 1/s |
| Sum of the squares of the residuals | 2,450 | 2,289 | m ² |

^a Averaged over 1937–1998 period

^b Averaged over length of fault

of the residuals also are provided, as calculated with Eq. (4). Figure 12 shows that the SSR is relatively insensitive to the return flow percentage, indicating that the agreement between the simulated and observed water levels is not significantly affected by the value of the return flow percentage. The results in Fig. 12 also indicate that the calibrated fault conductance increases as the return flow percentage decreases. This pattern reflects the notion that, as the effective pumping rate increases, more water has to flow from the Desert Hot Springs subbasin to the Mission Creek subbasin, where significantly more pumping is present. However, the range of values of the calibrated fault conductance indicated in Fig. 12 is relatively small, again indicating that the sensitivity of the model output and the calibrated parameters to return flow percentage is minimal.

The assumption that the outflows (eastern flux boundary outflow and Banning fault outflow) remain constant over the period of the transient calibration could also have an impact on the parameter estimates. Because these fluxes are essentially controlled by the magnitude of groundwater levels, it is possible that the outflows could change as groundwater elevations change, due to, for example, pumping. This assumption is tested by allowing the outflows to vary during the period of the transient phase calibration. The outflows are estimated for a series of six, 10-year intervals over the period 1937–1998.

The results of these simulations are shown in Fig. 13 and Table 5. Figure 13 shows that the estimated outflows vary significantly with time, in a pattern similar to that of the pumping in the respective basins (see Fig. 6). As indicated in Table 5, however, the average values of the outflows over the period 1937–1998 are similar to those estimated when the outflows were held constant. The re-estimated values of fault conductance (averaged along the length of the fault) also are similar to the values obtained when the outflows were held constant. However, the coefficients of correlation between the outflow parameter estimates and the storage coefficient are much higher in the case where the outflows were allowed to vary. Absolute values of the coefficients of correlation between the estimated storage coefficient and the estimated, time-varying outflows are on the order of 0.60–0.70, as compared to coefficients of correlation on the order of 0.30–0.40 obtained when the outflows were held constant. This result indicates that the factors responsible for transient changes in water level over the study period are not easily separated into changes in outflows and storage.

Summary

A conceptual and numerical model of a faulted, unconsolidated groundwater system was developed in an area at and near Desert Hot Springs, California. The groundwater system consists of two hydrologic subbasins (Desert Hot Springs and Mission Creek subbasins) bounded by the Mission Creek fault. The model development involved estimation of regional parameters—hydraulic conductivi-

ties and storage coefficients—and a parameter specific to the fault—the fault hydraulic conductance. The parameter estimation was based on calibrating the model with observed groundwater elevations from observation wells located at over 40 locations measured over a 60-year period.

The calibrated values of regional hydraulic conductivities and storage coefficient are reasonable, considering the aquifer materials found in the subbasins. The fault hydraulic conductance estimates yielded variations in the fault hydraulic conductance of about an order of magnitude along the fault length. The higher value of fault conductance in the southeastern portion of the fault was supported by hydraulic and geochemical observations. When an average fault thickness of 35 m is assumed, the fault hydraulic conductivity values are estimated to be from three to five orders of magnitude lower than the surrounding materials.

Sensitivity analysis indicates that assumptions made in the conceptual model, specifically the assumption that outflow rates remain constant over the study period (1936–1998) and the amount of pumped water returned to the subsurface, do not significantly affect estimated fault hydraulic conductances. However, field-based, direct estimates of parameters such as transmissivities in each subbasin and fault hydraulic conductances, would significantly improve confidence in the values of the parameters obtained by model calibration.

Acknowledgements The authors thank Dr. James Wood at Michigan Technological University (MTU) for the original suggestion to investigate the Mission Creek fault zone as a barrier to groundwater flow. The cooperation of the Mission Springs Water District (MSWD), Desert Hot Springs, California, especially Mr. John L. Morgan, has been essential to this study. The authors gratefully acknowledge the sources of funding for this study: the Petroleum Research Fund, MSWD, and MTU. Eric Reichard at the US Geological Survey (USGS) Water Resources Division office in San Diego, California was kind enough to provide historical data for pumpage and groundwater levels. Michael Rymer and Rufus Catchings of the USGS Earthquake Hazard Reduction office in Menlo Park, California provided interpretations of basement depths from their seismic-reflection surveys. Discussions with Dr. Jan Gillespie of the California State University, Bakersfield have been invaluable for refining the conceptual model of the groundwater-flow system.

References

- Bear J (1979) *Hydraulics of groundwater*. McGraw-Hill, New York
- Bense VF, Vanden Berg EH, Van Balen RT (2003) Deformation mechanisms and hydraulic properties of fault zones in unconsolidated sediments: the Roer Valley Rift System, The Netherlands. *Hydrogeol J* 11:319–332
- Bredhoeft JD, Belitz K, Sharp-Hansen S (1992) The hydrodynamics of the Big Horn Basin: a study of the role of faults. *AAPG Bull* 76:530–546
- Caine JS, Forster CB (1999) Fault zone architecture and fluid flow: insights from field data and numerical modeling, in faults and subsurface flow in the shallow crust. *AGU geophysical monograph*, vol 113. American Geophysical Union, Washington, DC
- Caine JS, Evans JP, Forster CB (1996) Fault zone architecture and permeability structure. *Geology* 24:1025–1028

- California Department of Water Resources (1964) Coachella Valley investigation: bulletin 108, CDWR, Sacramento, CA, USA
- California Department of Water Resources (1979) Coachella Valley area well standards investigation: southern district, CDWR, Sacramento, CA, USA
- Doherty J (1994) PEST, Watermark Computing, Corinda, Australia
- Ganser DR (1987) Hydrogeologic characteristics of the Ramapo fault, northern New Jersey. *Ground Water* 25:664–671
- Geotechnical Consultants, Inc. (1979) Hydrogeologic investigation-mission creek subbasin within the Desert Hot Springs County Water District, Geotechnical Consultants, Inc., Westerville, OH, USA
- Geotechnical Consultants, Inc. (1992) Groundwater resources: update, a Report for Mission Springs Water District, Summary of Findings and Conclusions with Recommendations, Desert Hot Springs, California, Geotechnical Consultants, Inc., Westerville, OH, USA
- Haneberg WC (1995) Steady-state groundwater flow across idealized faults. *Water Resour Res* 31:1815–1820
- Harding Lawson Associates (1985) Geothermal Resource Assessment and Exploration of Desert Hot Springs, Harding Lawson Associates, California, Novato, California
- Heynekamp MR, Goodwin LB, Mozley PS, Haneberg WC (1999) Controls on fault-zone architecture in poorly lithified sediments, Rio Grande Rift, New Mexico: implications for fault-zone permeability and fluid flow, faults and subsurface fluid flow in the shallow crust, geophysical monograph 113, American Geophysical Union, Washington, DC, pp 51–68
- Hsieh PA, Freckleton JR (1993) Documentation of a computer program to simulate horizontal-flow barriers using the US Geological Survey's Modular three-dimensional finite-difference ground-water flow model. *US Geol Surv Open-File Rep* 92-477
- Huntoon PW (1985) Fault severed aquifers along the perimeters of Wyoming artesian basins. *Ground Water* 23:176–181
- Huntoon PA, Lundy DA (1979) Fracture-controlled ground-water circulation and well siting in the vicinity of Laramie, Wyoming. *Ground Water* 17:463–469
- Kolm KE, Downey JS (1994) Diverse flow patterns in the aquifers of the Amargosa Desert and vicinity, southern Nevada and California. *Bull Assoc Eng Geol* 31:33–47
- Lines GC, Bilhorn TW (1996) Riparian vegetation and its water use during 1995 along the Mojave River, southern California. *US Geol Surv Water-Resour Invest Rep* 96-4241
- Lopez D, Smith L (1996) Fluid flow in fault zones: Influence of hydraulic anisotropy and heterogeneity on the fluid flow and heat transfer regime. *Water Resour Res* 32:3227–3238
- Lukkarila C (1999) Refinement of a groundwater flow model: upper Coachella Valley, Riverside County, California, MSc Thesis, Michigan Technological University, Houghton, MI, USA
- Marler J, Ge S (2003) The permeability of the Elkhorn Fault Zone: a case study from South Park, Colorado. *Ground Water* 41:321–332
- May WL (1996) Characterization of a large fault zone as a barrier to fluid flow, San Andreas Fault, near Desert Hot Springs, Riverside County, California. MSc Thesis, Michigan Technological University, Houghton, MI, USA
- Mayer AS, May WL (1998) Mathematical modeling of proposed artificial recharge of the Mission Creek Subbasin. Dept. of Geological Engineering and Sciences. Michigan Technological University, Houghton, MI, USA
- McDonald MG, Harbaugh AW (1988) A modular three-dimensional finite-difference ground-water flow model In: *US Geological Survey Techniques of Water Resources Investigations, Book 6, Chapter A1*, US Geol Surv, Reston, VA, USA
- Mozley PS, Davis JMD (1996) Relationship between oriented calcite concretions and permeability correlation structure in an alluvial aquifer, Sierra Ladrones Formation, New Mexico. *J Sediment Res* A66:11–16
- Mozley PS, Goodwin L (1995) Patterns of cementation along a Cenozoic normal fault: a record of paleoflow orientations. *Geology* 23:539–542
- Mozley PS, Beckner J, Whitworth TM (1995) Spatial distribution of calcite cement in the Santa Fe Group, Albuquerque Basin, NM: implications for groundwater resources. In: *Spec Issue: Albuquerque Basin: studies in hydrogeology*. *New Mexico Geol* 17:88–93
- Proctor RJ (1968) *Geology of the Desert Hot Springs-Upper Coachella Valley Area, Special Report 94*, California Division of Mines and Geology, Sacramento, CA
- Rasmussen GS (1979) *Engineering Geology Investigations, project #1430, 100-acre parcel, North of Dillon Rd., East of Long Canyon Rd., Desert Hot Springs, CA*, Gary S. Rasmussen and Associates, San Bernardino, CA, USA
- Reichard EG, Meadows JK (1992) Evaluation of a ground-water flow and transport model of the Upper Coachella Valley, California, *US Geol Surv Water-Resour Invest Rep* 91-4142
- Seber GAF, Wild CJ (1989) *Nonlinear regression*. Wiley, New York, p 768
- Sigda JM, Goodwin LB, Mozley PS, Wilson JL (1999) Permeability alteration in small-displacement faults in poorly lithified sediments: Rio Grande Rift, Central New Mexico. In: *Faults and subsurface fluid flow in the shallow crust, Geophysical Monograph 113*, American Geophysical Union, Washington, DC, pp 51–68
- Smith L, Forster C, Evans J (1990) Interaction of fault zones, fluid flow, and heat transfer at the basin scale. In: Neuman SP, Neretnieks I (eds) *Hydrogeology of low permeability environments*. Verlag Heinz Heise, Hanover, Germany, pp 41–67
- Swain LA (1978) Predicted water-level and water quality effects of artificial recharge in the Upper Coachella Valley, California, using a finite element digital model. *US Geol Surv Water-Resour Invest Rep* 77–29
- Tyley SJ (1971) Analog model of the ground-water basin of the Upper Coachella Valley, California. *US Geol Surv Open-File Rep* 7417-03
- Tyley SJ (1974) Analog model study of the ground-water basin of the Upper Coachella Valley, California. *US Geol Surv Water-Suppl Pap* 2027
- Vander Velpen BPA, Sporry RJ (1993) Resist: a computer program to process resistivity sounding data on PC compatibles. *Comput Geosci* 19:691–703
- Zhody AAR, Eaton GP, Mabey DR (1974) Application of surface geophysics to ground-water investigations. *Techniques of water-resources investigations of the United States Geological Survey, Chapter D1*, US Geological Survey, Reston, VA, USA